



Effect of Nb and Ta addition on mechanical properties of Zr-based bulk metallic glasses and composites

Ziyun Long^a, Pingjun Tao^{a,*}, Guotai Wang^a, Kunsen Zhu^a, Yugan Chen^a, Weijian Zhang^a, Zhihao Zhao^a, Yuanzheng Yang^a, Zhenghua Huang^b

^a School of Materials and Energy, Guangdong University of Technology, Guangzhou 510006, China

^b Guangdong – Hong Kong Joint Research and Development Center on Advanced Manufacturing Technology for Light Alloys, Institute of New Materials, Guangdong Academy of Sciences, Guangzhou 510650, China



ARTICLE INFO

Article history:

Received 21 December 2021

Received in revised form 9 April 2022

Accepted 15 April 2022

Available online 21 April 2022

Keywords:

Bulk metallic glasses

Mechanical properties

Shear bands

Microalloying

ABSTRACT

To modify the poor plasticity of bulk metallic glasses (BMGs) under room temperature, the present work reported that microalloying can improve the plasticity of BMGs, and the deformation mechanism at room temperature was elucidated. The selection of minor elements, Nb and Ta have a positive heat of mixing with the based compositions. The maximum plasticity of 32.9% is shown in the Nb1 sample. The self-organize to a critical state (SOC) occurred in all BMGs, the scaling exponent β value maintains the constant 0.24. The variation of the rotation angle of primary shear bands (SBs) is in agreement with plasticity. Meanwhile, the yield strength is linearly dependent on the local fracture toughness of BMGs. Summarily, the compressive plasticity of BMGs at room temperature can be improved by adding elements that can form positive mixing heat with the components of based compositions.

© 2022 Elsevier B.V. All rights reserved.

1. Introduction

Bulk metallic glasses (BMGs) have attracted wide attention from researchers due to their excellent mechanical, chemical, and physical properties, including prominent biological compatibility, relatively low elasticity modulus, large fracture strength, and corrosion resistance [1–10]. As we all know that the atoms are arranged chaotically in BMGs contributing to disorder in the long-range and order in the short-range, and plastic deformation is related to nano-scale shear bands (SBs) [11,12], and then catastrophic fracture occurs through the expansion of rapid multiplication of SBs [13,14]. Zr-based BMGs are a kind of highly promising engineering structural materials with great commercial applications and they have excellent superplasticity in the supercooled liquid region (SLR), but their depleted plasticity at room temperature has hampered their widespread application [15,16]. Improving the plasticity and understanding the deformation mechanism at room temperature of Zr-based BMGs have become the main challenges in the underlying field.

There are a series of methods to improve the plasticity of BMGs. For instance, Zhao et al. [4] investigated the microalloying of oxygen

whose plasticity was improved from 5.3% to 12.3% when oxygen content increased from 0% to 2.87%. Luo et al. [17] utilized hydrogen microalloying to enhance the plasticity of Zr-based BMGs. Ding et al. [18] studied that Ti addition significantly improved the plasticity and fracture strength of $Zr_{54}Al_{10.2}Ni_{9.4}Cu_{26.4}$ BMG. Guo and Li [19] investigated the effect that cryogenic thermal cycling induced more disordered high-energy states in structure, which corresponds to a production of excess free volume and therefore modifies the plasticity of BMGs. Zhang et al. [20] demonstrated that prolonged elastostatic compression imposed on metallic glasses at room temperature induced homogenous deformation associated with structural disordering, which enhances the plasticity of BMGs. Therefore, how to improve the plastic strain of BMGs is still an open issue. To date, however, how to obtain an efficient and low-cost process technique to improve the plasticity of Zr-based BMGs at room temperature is currently a key research challenge.

In our work, we investigate the poor plasticity of Zr-based BMGs at room temperature by adding minor alloying elements in an attempt to improve the room temperature plasticity of Zr-based BMGs and to promote the industrial application of Zr-based BMGs. Enhancing the plasticity of BMGs via minor elements addition is an effective method. But few studies reported the effect of adulterated minor elements on the plasticity, it maintains unclear how doping factors affect the plastic strain of BMGs. The chemical structural heterogeneity would be induced when appearing positive heat of

* Corresponding author.

E-mail address: pjtao@gdut.edu.cn (P. Tao).

Table 1

The heat of mixing (ΔH_{A-B}) between the additional elements and different compositions (kJ/mol) [22].

compositions	Zr	Ni	Al
Cu	-23	4	-1
Nb	10	-30	-38
Ta	3	-29	-19

mixing between the minor elements and main elements, e.g., introducing the crystallization phases, and formation of structural inhomogeneity. Therefore, understanding the chemical structural heterogeneity of BMGs is of great importance to guide the preparation of BMGs with high plasticity at room temperature. In this article, the plastic strain can be enhanced in the $Zr_{60}Cu_{20}Al_{10}Ni_{10}$ BMG [21] by adding minor elements, compared to the primitive. To obtain high structural heterogeneity and thus increase the plasticity of Zr-based BMGs at room temperature, and considering the heat of mixing between the doping elements and the compositions Zr, Ni, and Al (listed in Table 1), we investigated the correlation of plasticity with structure feature variation in Zr-Cu-Al-Ni BMGs by substituting part of Cu with Nb and Ta. Meanwhile, the mechanical properties and fracture mechanisms of the BMGs are discussed.

This research has enabled us to obtain a convenient, effective, and inexpensive technique for enhancing the plasticity of BMGs and to develop Zr-based BMGs' compositions with excellent plasticity at room temperature, accelerating the application of Zr-based BMGs in engineering materials field. In addition, the deformation pattern of Zr-based BMGs is investigated by microalloying, and the deformation mechanism of Zr-based BMGs at room temperature is revealed.

2. Experimental

The nominal composition $Zr_{60}Cu_{20-x}Al_{10}Ni_{10}M_x$ ($M = Nb$ and Ta , $x = 0, 1, 3$, and 5 , denoted as M0, Ta1, Ta3, Ta5, Nb1, Nb3, and Nb5, respectively) were prepared by arc melting mixtures of the constituent elements with a purity of above 99.9% under a Ti-getter argon atmosphere. The alloy ingots must be remelted at least four times to ensure compositional homogeneity. Seven master alloy rod specimens with 3 mm in diameter and 80 mm in length were fabricated by copper mold suction casting method in the high pure argon atmosphere. The compressive specimens were incised to 4.5 mm-length with an aspect ratio of 1.5:1 by a wire-cut electrical discharge machine. Both the two sections of the specimens were paralleled by carefully grinding and polishing.

The structures of the as-cast alloys $Zr_{60}Cu_{20-x}Al_{10}Ni_{10}M_x$ ($M = Nb$ and Ta , $x = 0, 1, 3$, and 5) were detected by X-ray diffraction (XRD, D/Max-Ultima IV) with $Cu K\alpha$ radiation. The thermal behaviors of the specimens were investigated by different scanning calorimetry (DSC, PerkinElmer DSC800) under a continuous N_2 flow at a heating rate of $20\text{ }^{\circ}\text{C}/\text{min}$. Scanning electron microscope (SEM, S-3400N) was carried out to verify the fracture morphologies of specimens. The hardness was studied by a micro-Vickers hardness tester (HVS-1000Z). The quasi-static uniaxial compressions of specimens were performed with an AG-X plus electronic universal testing machine under a strain rate of $5 \times 10^{-4}/\text{s}$ at room temperature. Every composition must measure three times for the compression test to ensure the repeatability and reliability of the experiment data.

3. Results

3.1. Microstructural characterization of the $Zr_{60}Cu_{20-x}Al_{10}Ni_{10}M_x$ alloys

The microstructural characterization of the $Zr_{60}Cu_{20-x}Al_{10}Ni_{10}M_x$ alloys has been verified by X-ray diffraction and the patterns are shown in Fig. 1. It can be seen that there is exhibited only a diffuse

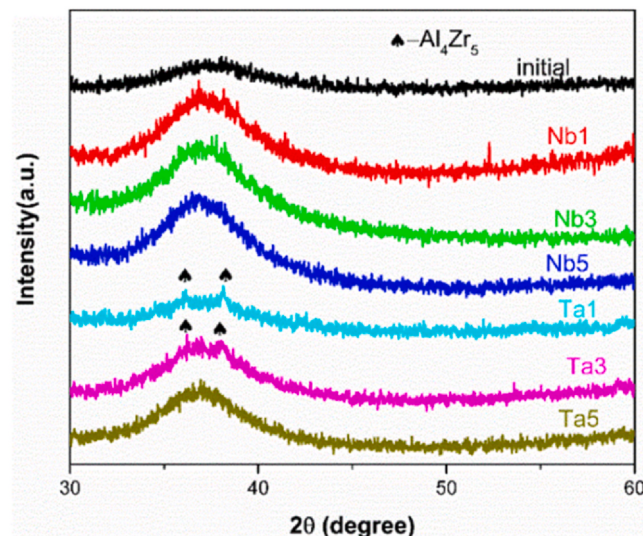


Fig. 1. XRD patterns of the $Zr_{60}Cu_{20-x}Al_{10}Ni_{10}M_x$ BMGs with a diameter of 3 mm.

peak in the range of $2\theta = 30\text{--}40^{\circ}$ for the Nb addition and the Ta content of 5 (at%) of the alloy specimens, which implies the amorphous feature of those specimens. However, it is expressed the crystal peaks corresponding to the crystallization phase for the specimens of Ta content of 1 and 3 (at%), suggesting that a part of metallic glass will crystallize when the minor element Ta addition content of 1 and 3 (at%).

3.2. Thermodynamic behavior of the $Zr_{60}Cu_{20-x}Al_{10}Ni_{10}M_x$ alloy specimens

DSC measurements were carried out at a constant heating rate of $20\text{ }^{\circ}\text{Cmin}^{-1}$ and the DSC curves of $Zr_{60}Cu_{20-x}Al_{10}Ni_{10}M_x$ alloy specimens are presented in Fig. 2. There is an exothermic peak for the glass transition process as the result of the structure relaxation releasing the free volume to approach equilibrium during the continuous heating [23], and the subsequent exothermic peak of the crystallization process for each specimen. It can be seen that there is only an exothermic peak of crystallization in the Nb and Ta addition content of 1 and 3 (at%), the multiple crystallization peak emerged in

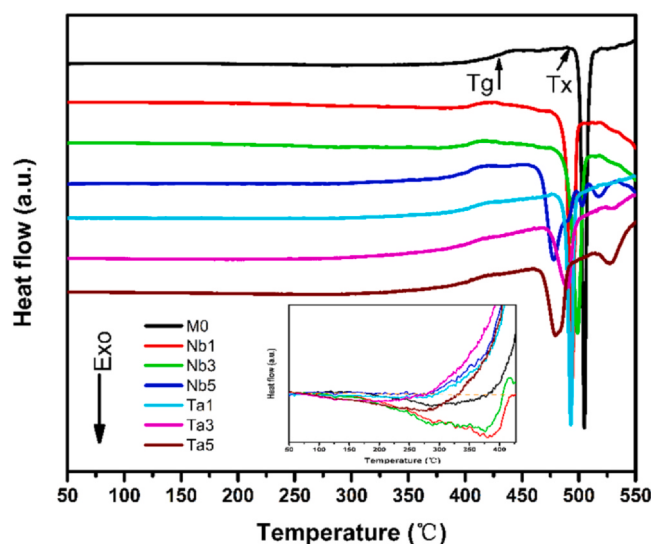


Fig. 2. The DSC curves of the $Zr_{60}Cu_{20-x}Al_{10}Ni_{10}M_x$ BMGs at a heating rate of $20\text{ }^{\circ}\text{Cmin}^{-1}$.

Table 2

The thermodynamic characteristic of the $Zr_{60}Cu_{20-x}Al_{10}Ni_{10}M_x$ ($M=Nb$ and Ta , $x=0, 1, 3$, and 5) BMGs with the measured T_g , T_x , ΔT_x , ΔH , and ΔH_r .

Materials	T_g (°C)	T_x (°C)	ΔT_x (°C)	ΔH (J/g)	ΔH_r (J/g)
M0	427	501	74	51.27	3.27
Nb1	409	490	84	55.93	7.57
Nb3	405	492	87	59.04	6.13
Nb5	404	467	63	53.83	1.52
Ta1	406	489	83	49.61	2.36
Ta3	407	474	67	41.22	2.49
Ta5	405	468	63	45.78	5.29

the Nb and Ta content of 5 (at%), which indicated multiple-steps crystallization behavior for one crystallization procedure. The feature temperatures of glass transition temperature T_g , and onset crystallization temperature T_x , can be seen distinctly in the DSC traces of those alloy specimens. The crystallization enthalpy ΔH and the supercooled liquid region range ΔT_x ($T_x - T_g$) are determined and listed in Table 2. It is the case that the supercooled liquid region ΔT_x is increasing at first and then decreasing for Nb-containing, and decreasing continuously by increasing the addition content of Ta. On the contrary, the crystallization enthalpy is decreasing at first and then increasing with increasing Nb content. The opposite is true for those Ta-containing specimens. Meanwhile, the relaxation enthalpy ΔH_r is also calculated.

3.3. Mechanical properties of the $Zr_{60}Cu_{20-x}Al_{10}Ni_{10}M_x$ alloy specimens

Uniaxial compression tests were carried out at the strain rate of 5×10^{-4} /s. Fig. 3(a) exhibited the typical compression stress versus strain curves of the different compositions of the $Zr_{60}Cu_{20-x}Al_{10}Ni_{10}M_x$ alloy specimens at room temperature. The

Table 3

The plasticity, yield strength, fracture strength, and hardness of $Zr_{60}Cu_{20-x}Al_{10}Ni_{10}M_x$ alloy specimens at room temperature compression.

Material	Plasticity	Yield strength (MPa)	Fracture strength (MPa)	Hardness (HV)
M0	0.057 ± 0.007	1708 ± 75	1804 ± 2	524.8 ± 19
Nb1	0.329 ± 0.035	1305 ± 143	2142 ± 118	445.7 ± 9.1
Nb3	0.117 ± 0.038	1491 ± 34	1792 ± 68	444.3 ± 8.7
Nb5	0.152 ± 0.022	1538 ± 125	1870 ± 49	443.0 ± 10.5
Ta1	0.026 ± 0.001	919 ± 140	1083 ± 122	490.8 ± 10.0
Ta3	0.067 ± 0.011	1012 ± 64	1108 ± 10	487.6 ± 13.0
Ta5	0.096 ± 0.014	1178 ± 51	1448 ± 13	498.4 ± 12.2

plasticity, yield strength, fracture strength, and hardness were measured and shown in Table 3, and the mechanical properties graph of Nb and Ta addition were plotted in Fig. 3(b) and Fig. 3(c), respectively. For the Nb addition alloy specimens, the plasticity and fracture strength are first increasing and then decreasing with adding the Nb content. Relative to the Ta addition, the plasticity, yield strength, and fracture strength are enhanced continuously with increasing Ta content. The specimens at Nb content of 1 (at%) exhibited maximum plasticity of 32.9%. On the contrary, only 2.6% of plastic strain for 1 (at%) Ta content. All the plasticity has been enhanced for Nb minor element addition but the yield strength is lowered. For the Ta addition, all of the strength is decreased but the plastic strain has been modified when Ta content of 3–5 (at%). The Nb addition decreases the hardness of specimens, and decreases at first and then the enhancement of hardness for increasing Ta content.

Figs. 4 and 5 represented the side-face morphology and fractography of the $Zr_{60}Cu_{20-x}Al_{10}Ni_{10}M_x$ alloy specimens after compression failure. Some of the SBs appeared on the studied specimens, and

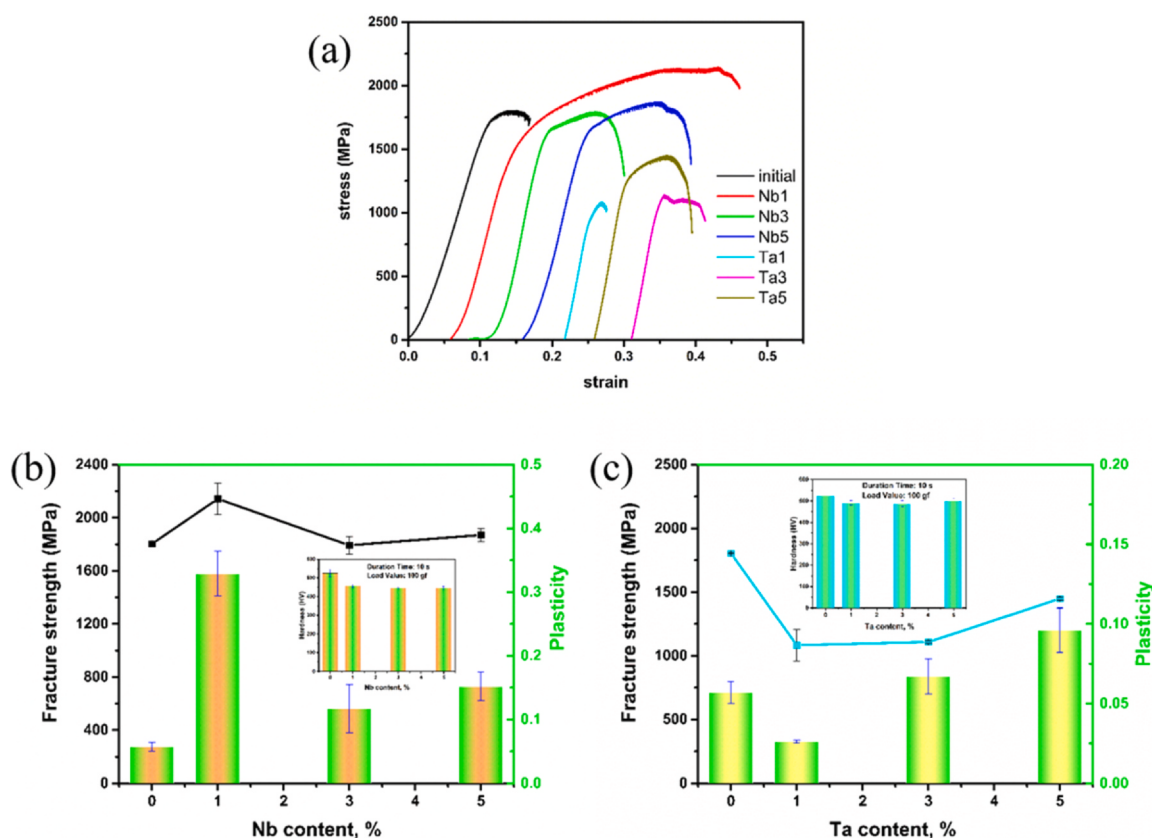


Fig. 3. (a) Room-temperature compression engineering stress-strain curves of $Zr_{60}Cu_{20-x}Al_{10}Ni_{10}M_x$ alloy specimens; The fracture strength, plasticity, and hardness of the specimens of adding the minor elements of (b) Nb and (c)Ta.

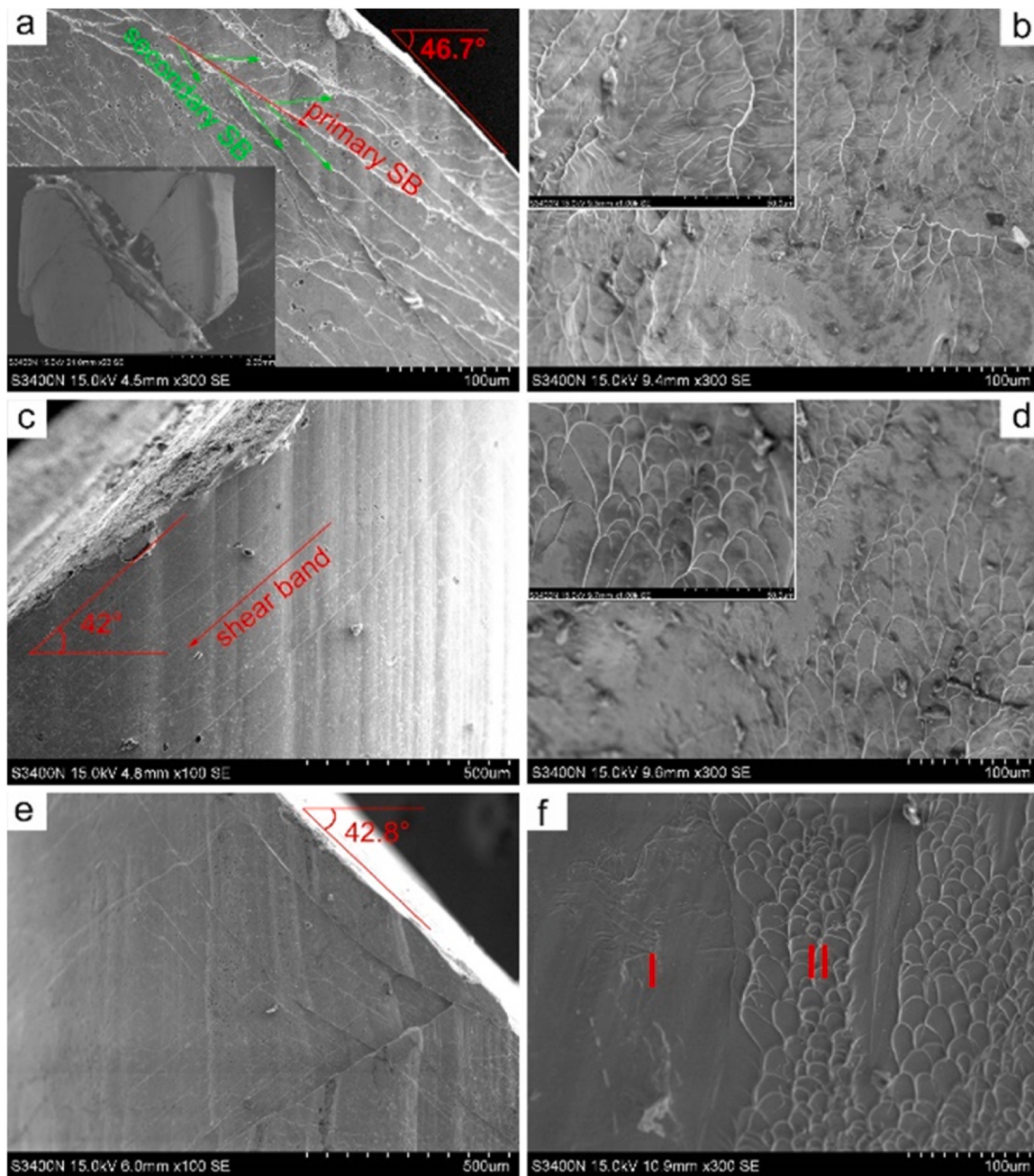


Fig. 4. The SEM images of the section surface morphology and fractographies of $Zr_{60}Cu_{20-x}Al_{10}Ni_{10}Nb_x$ alloy specimens: (a-b) Nb1; (c-d) Nb3; (e-f) Nb5.

the distribution on the Nb1, Nb5, and Ta5 were occurring bifurcation and crisscross, the SBs of Nb3 and Ta1 are parallel. In the fractography, the Nb1 specimen emerges the vein-like patterns and other samples appear the scale-like patterns. The plasticity is revealed via the competitive relationship between the pattern region and the smooth region. With increasing the Nb content, the patterns from vein-like to scale-like and the pattern regions increase.

4. Discussion

In general, the addition of minor elements can enhance the plasticity of Zr-based BMGs at room temperature. Liu et al. [24] clarified that the plasticity was enhanced with increasing Nb content. Li et al. [25] demonstrated that the Ta addition can increase the plasticity of Zr-based BMG. In this section, we discuss the effect of Nb and Ta on the thermodynamic behavior and mechanical

properties of $Zr_{60}Cu_{20}Al_{10}Ni_{10}$ BMG. Simultaneously, we also revealed the deformation mechanism of the BMGs at room temperature.

4.1. The effect of Nb and Ta addition on microstructure and thermodynamic behavior

Fig. 1 shows that the Nb-doped alloy is fully amorphous, while the Ta content of 1 at% and 3 at% is partially crystalline. For the bonding nature between the M element doping and the base constituent elements (Zr, Cu, Ni, and Al), Nb-Zr, Ta-Zr, and Ta-Cu form strong repulsive states, but atom pairs with other atoms are strongly attractive bonding nature [26]. These strong atom pairs tend to form dense stacks and thus enhance amorphous formation. Since the atomic radii of both Nb and Ta are larger than those of Cu, by Eq. (1) [27]:

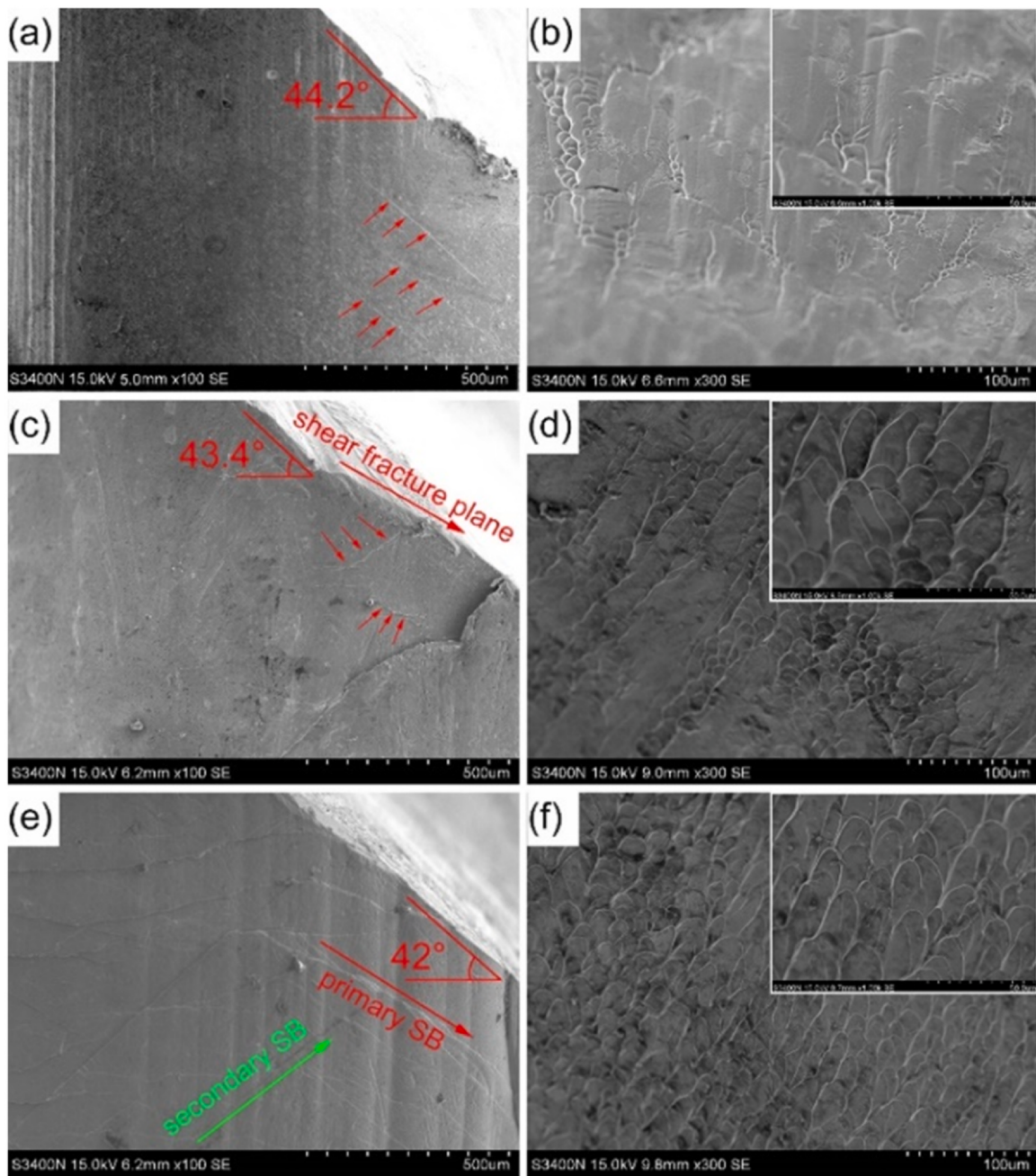


Fig. 5. The SEM images of the section surface morphology and fractographies of $Zr_{60}Cu_{20-x}Al_{10}Ni_{10}Ta_x$ alloy specimens: (a-b) Ta1; (c-d) Ta3; (e-f) Ta5.

$$N^T = \begin{cases} \frac{4\pi}{6\arccos\left\{\sin\left(\frac{\pi}{3}\right)\left[1 - \frac{1}{(R+1)^2}\right]^{\frac{1}{2}}\right\} - \pi} & \text{for } 0.225 \leq R < 0.414, \\ \frac{4\pi}{8\arccos\left\{\sin\left(\frac{\pi}{4}\right)\left[1 - \frac{1}{(R+1)^2}\right]^{\frac{1}{2}}\right\} - 2\pi} & \text{for } 0.414 \leq R < 0.902, \\ \frac{4\pi}{10\arccos\left\{\sin\left(\frac{\pi}{5}\right)\left[1 - \frac{1}{(R+1)^2}\right]^{\frac{1}{2}}\right\} - 3\pi} & \text{for } R \geq 0.901, \end{cases} \quad (1)$$

where N^T is theoretical coordination number, R is radius ratio, $R = r_i/r_j$, r_i is the clusters central circle atoms radius, and its first-nearby neighbors atoms radius r_j . This theoretical nearest-neighbor coordination number on Cu-, Nb- and Ta- centered were shown in Table 4. Variation of system mixing enthalpy with replacement

Table 4

Atomic radius r , radius ratio R , theoretical coordination number N^T , the most possible coordination number N [27].

elements	r (Å)	R	N^T	N
Zr	1.58			
Cu	1.27	0.803	10.05	10
Nb	1.46	0.924	12.29	12
Ta	1.49	0.943	12.55	12

element content shown in Fig. 6. For the Nb substitution, a fully amorphous structure was formed due to its strong bonding with Cu, Al and Ni and the formation of clusters with Zr that are more densely packed than Cu, which combine to counteract the effect of the reduced negative mixing enthalpy. For Ta substitution, the clusters formed with Zr are more densely packed than Cu-Zr, and as the Ta content increases, the promotion effect of the dense packing

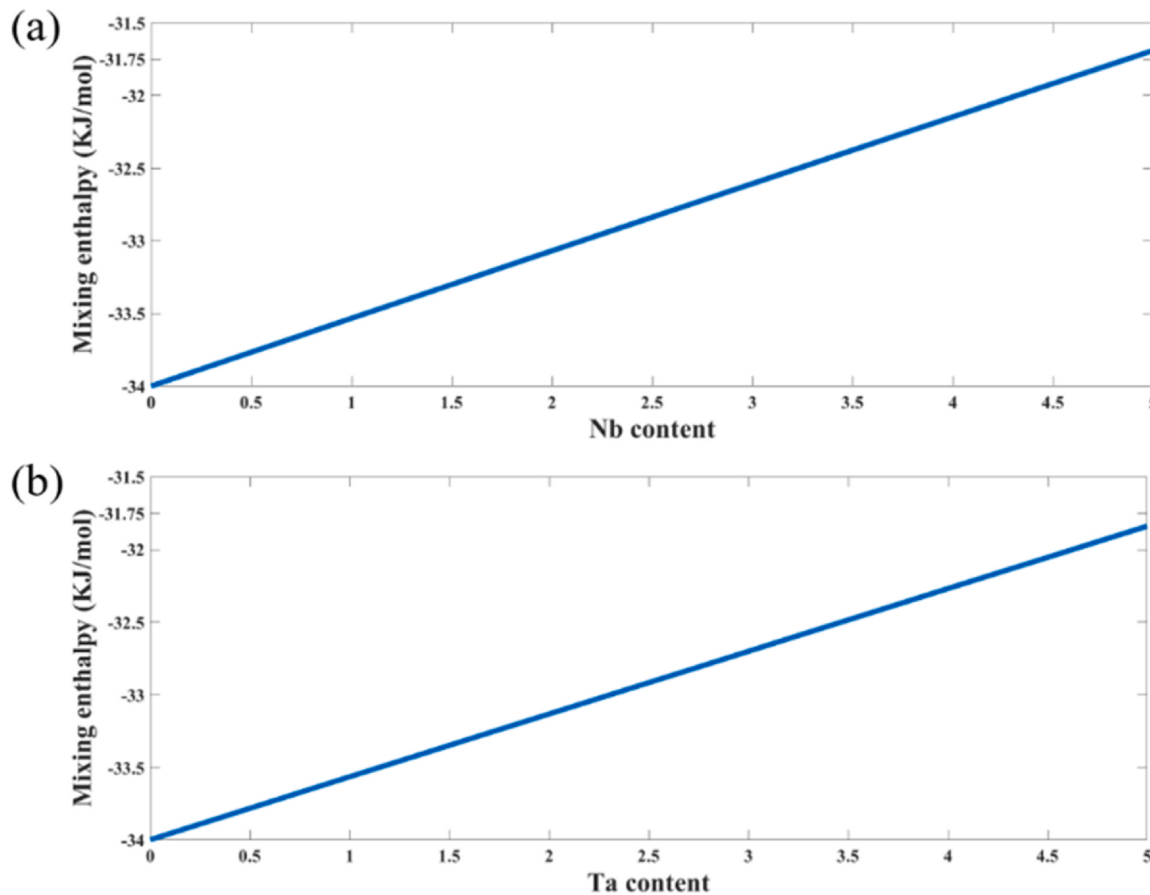


Fig. 6. Variation of system mixing enthalpy with replacement element content: (a) Nb; (b) Ta.

counteracts the negative mixing enthalpy reduction, so the change from partially crystalline to fully amorphous.

Fig. 2 shows the traces of thermodynamic properties for the $Zr_{60}Cu_{20-x}Al_{10}Ni_{10}M_x$ specimens. There is a clear peak for all specimens before the glass transition temperature corresponding to the structure relaxation, due to the release of the free volume to approach the equilibrium value, as shown in Fig. 2 illustration. This process of structure relaxation is when the free volume annihilates and produces to approach the equilibrium [22]. The T_g and T_x of the specimens shift to low temperature when adding the Nb and Ta. The T_g is increasing and then decreasing and T_x is only decreasing with increasing Ta content. Compared to Nb, the T_g is merely decreasing and the T_x is decreasing after first increasing. In addition, the ΔT_x is a similar trend with T_x for Nb addition but continuously decreases for the addition of Ta, which indicated the thermostability of the glass phase is decreasing for Ta addition. Inoue [28] indicated that the broader supercooled liquid region is the symbolism of more stable amorphous alloys, the crystallization of Ta addition due to occur chemical heterogeneity to deviate the compositions of high GFA. The multiple crystallization occurs at $450 \sim 550^\circ\text{C}$ in the specimens of Nb5 and Ta5. It means that different crystallization phases can be obtained by controlling the annealing temperature. Meanwhile, the crystallization and relaxation enthalpies are calculated. The crystallization enthalpy attributes to the formation of critical nucleation [29]. The relaxation is correlated with the free volume. In this literature, the trend of relaxation enthalpy is different from the plasticity of BMGs, indicating that the free volume is not the domination for the plastic strain of BMGs of microalloying.

4.2. The effect of mechanical properties with Nb and Ta addition

Structural heterogeneity is closely related to the characteristic free volume of structural relaxation [30]. The more free volumes in a BMG system, the more structural heterogeneity increases. The relationship between relaxation enthalpy ΔH_r and the free volume change per atomic volume, Δv_r , can be expressed as [23]:

$$\Delta H_r = \alpha \cdot \Delta v_r \quad (2)$$

where α is a constant. Therefore, the free volumes can be characterized by the relaxation enthalpy. For Nb1, Nb3 and Ta5, the relaxation enthalpies were larger than the original, so their free volumes were more, i.e., the heterogeneity within their systems is more pronounced. Therefore, the addition of Nb and Ta is beneficial in inducing heterogeneity in BMGs.

For the large variability of plasticity at room temperature between Nb1 and Ta1, the reason is attributed to structural heterogeneity. For Nb1, the internal free volumes increased due to its chemical structural heterogeneity. According to the shear transformation regions (STZs) model, the free volumes will act as a nucleation site for the SBs and impede the propagation of the SBs [31], leading to the creation of multiple SBs and thus increasing plasticity. For Ta1, the crystalline phase is Al_4Zr_5 . When it is subjected to external loading, the SBs generated in the glass matrix regulate the plasticity of the composite before the crystalline phase undergoes brittle fracture. The softening then induces failure to occur. Furthermore, the crack tip occurs preferentially in the crystalline phase, which then expands to guide the amorphous matrix, leading to premature failure of this amorphous alloy composite [32].

SB is a common plastic deformation characterization in BMGs. SB plays a crucial role in the plasticity and fracture of BMGs at room temperature [33]. To further understand the relationship between various structures and mechanical properties, the part of Cu is substituted by the congeneric element Nb and Ta to investigate the variation of the chemical structural heterogeneity and evolution of SBs with increasing contents of addition. The compression plasticity of BMGs was detected by a universal testing machine at room temperature. Corresponding varies of SBs and morphologies during deformation and failure were observed by SEM.

The compression stress vs. strain traces for the specimens are exhibited in Fig. 3(a). The serration process exhibits the repeating cycle of stress ups and downs under reloading elastically (show Fig. 6a). To further investigate the serration events which include an elastic energy accumulation and release process, the elastic energy density of one serration event ($\Delta\delta$) as [34,35]:

$$\Delta\delta = \frac{1}{2}\Delta\sigma_E\Delta\varepsilon_E \quad (3)$$

where $\Delta\sigma$ and $\Delta\varepsilon$ are the elastic stress and elastic strain of one serration, respectively. The ergodic processing of elastic energy density shows a cumulative probability distribution (see Fig. 6). The cumulative probability distribution can be approximated well as a power-law distribution function accompanied with squared exponential decay function [28]:

$$P(\geq\Delta\delta) = A\Delta\delta^{-\beta}\exp\left[-\left(\frac{\Delta\delta}{\delta_c}\right)^2\right] \quad (4)$$

where A is a normalization constant, β is a scaling exponent, and δ_c is the cut-off elastic energy density. The fitting parameters for the seven BMGs are listed in Table 5. The three parameters, β , $\Delta\delta$, and δ_c provide a fingerprint reflecting the dynamics of shear deformation in BMGs. The β values are maintained range of 0.22–0.24. The universal exponent of 0.24 in different compositions indicated that serrated flow behavior is a self-organization to a critical state (SOC) behavior [34]. The δ_c value represent the characteristic parameter related to the microstructural characteristic scale, which corresponded to the characteristic of shear size of the BMGs. And the $\Delta\delta$ value is associated with the amount of the STZs motion. (Fig. 7)

A usual fracture characteristic of the seven BMGs is that the final failure always abides by a shear pattern. In Figs. 4 and 5, the final fracture angle θ_c^F can be observed. A strong intersection between the primary and secondary SBs appeared in the Nb1, Nb5 and Ta3, but the SBs are rarely emerging in Ta1 and Ta3. Zhang et al. [36] considered that secondary SBs can contribute to the rotation of the primary SBs. For a better describing the relationship between the shear failure and the rotation mechanism of primary SBs, the function of the relationship among initial angle θ_c^0 , θ_c^F , and the plasticity ε_p described as [36]:

$$\sin(\theta_c^0) = (1 - \varepsilon_p)^{\frac{1}{2}}\sin(\theta_c^F) \quad (5)$$

This means that one can be approximately calculated the initial angle of primary SBs if the final fracture angle and plasticity were known. Then, the rotation angle ($\theta_c^F - \theta_c^0$) was also determined, as listed in Table 5. The rotation angle variation trend is agreeing with the plastic strain of the BMGs, and the rotation angle is linearly dependent on the value of plasticity, as show in Fig. 8(a). Apparently, the high compressive plastic strain corresponds to a large rotation angle. The addition of Nb significantly increases the rotation angle of the primary SBs. But when Ta is added, the rotation angle decreases when the addition amount is 1 at% and increases the addition amount of Ta, the rotation angles become larger. This is attributed to the crystallization of the Ta1 and Ta3 samples, which hinders the slip of the primary SBs and allows them to deflect at smaller angles.

Table 5
Scaling exponent (β), cut-offs for the elastic energy density (δ_c), normalization constant (A), final shear fracture angle (θ_c^F), initial shear angle (θ_c^0), rotation angle ($\theta_c^F - \theta_c^0$) (°), fracture toughness (K_C).

BMGs	β	δ_c (Jm ⁻³)	A	θ_c^F (°)	θ_c^0 (°)	$(\theta_c^F - \theta_c^0)$ (°)	K_C (MPa m ^{1/2})
M0	0.24	19,571	4.8	45.9	44.2	1.7	34.65
Nb1	0.24	9907	5.5	46.7	36.6	10.1	26.08
Nb3	0.24	4710	4.3	42.0	39.0	3.0	31.42
Nb5	0.24	9217	3.8	42.8	38.7	4.1	33.94
Ta1	0.22	4778	4.0	44.2	43.5	0.7	12.20
Ta3	0.23	2796	4.5	43.4	41.6	1.8	19.74
Ta5	0.23	5866	4.9	42.0	39.5	2.5	25.94

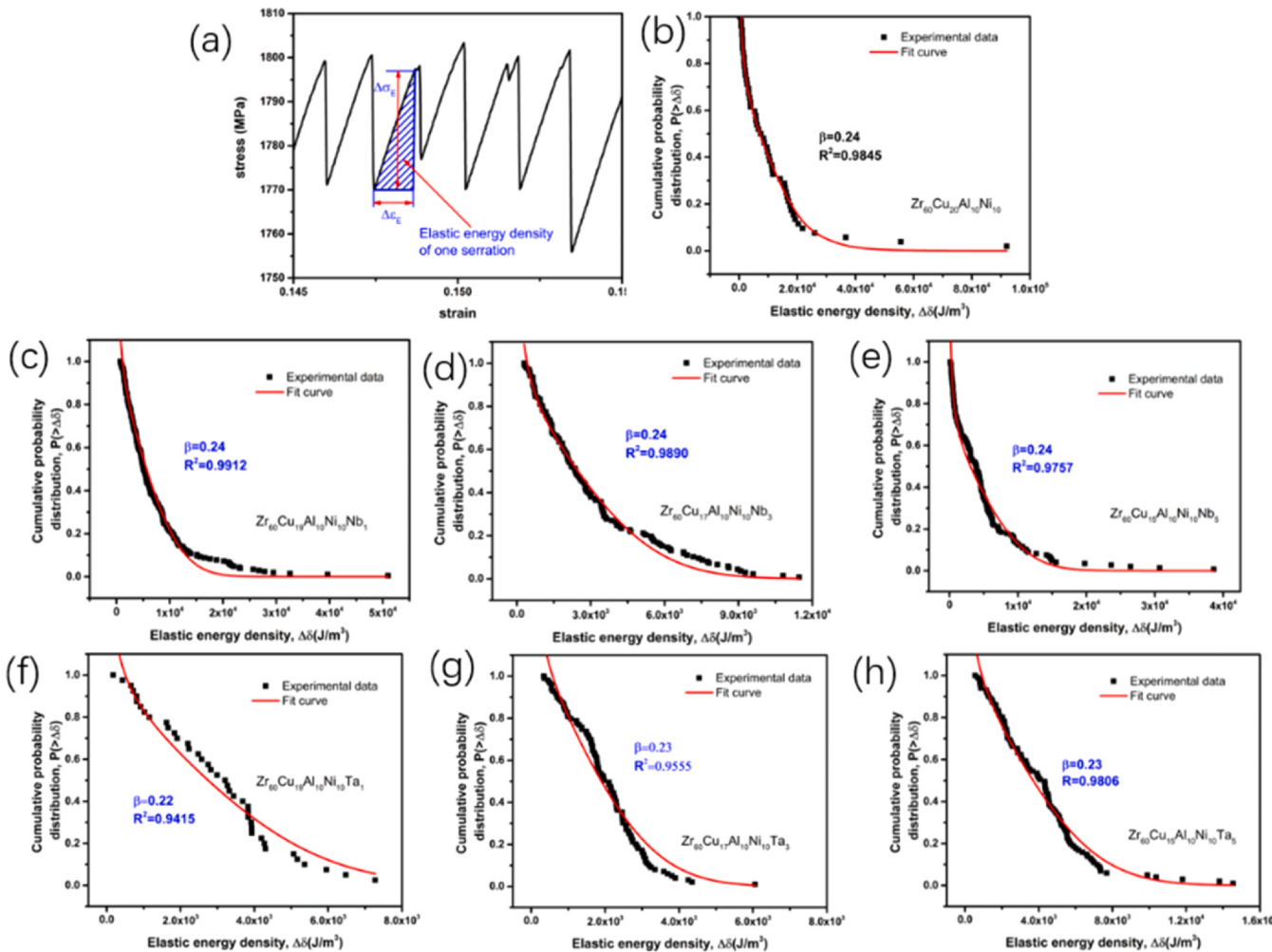


Fig. 7. (a) Elastic energy density for one serration. (b-h) The cumulative probability distribution for the elastic energy densities of seven BMGs. The scattering points are the experimental data and the red solid lines are fitted by Eq. (2).

Figs. 4 and 5 also exhibit atypical fracture surfaces, and the mirror region (region I) and the pattern region (region II) are shown in Fig. 4(f). The mirror region of Nb5 and Ta1 appears remarkably flat and shining, indicating slow crack propagation. Previous investigations manifest local plastic region in the fracture surface has a strikingly similar shape but at different scales [37]. Using the function of the local plastic region to calculate the fracture toughness (K_C) from the following equation [37,38]:

$$K_C = \sigma_y (6\pi w)^{1/2} \quad (6)$$

where σ_y and w are yield strength and length scale of the plastic region, respectively. The estimated fracture toughness is summarized in Table 5 and Fig. 8(b). This local fracture toughness is approximately linearly distributed with the yield strength of the BMGs. Therefore, the yield strength of BMGs with large fracture toughness is also high, and vice versa. When Nb and Ta are added, the fracture

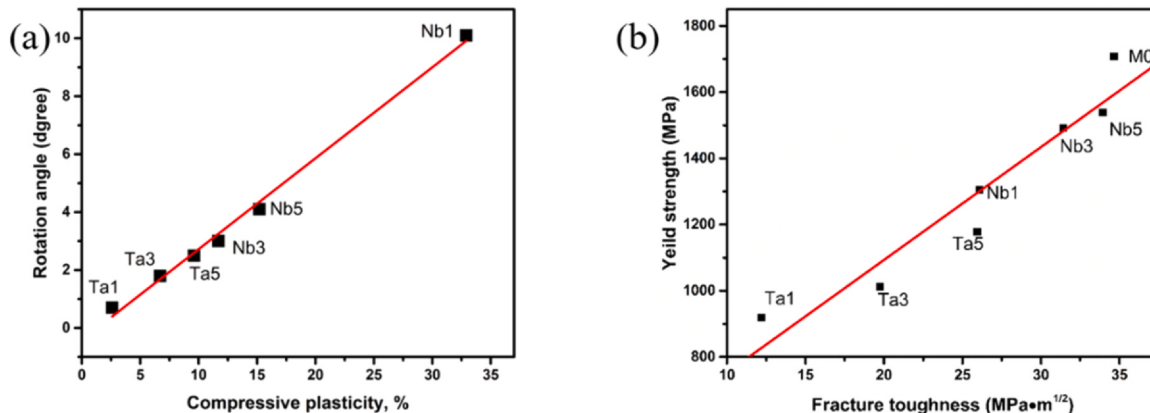


Fig. 8. (a) Dependence of the rotation angle on the applied compressive plasticity. (b) The variation of yield strength corresponds to the fracture toughness.

toughness of the BMGs decreases. The fracture toughness of Nb-containing BMGs is higher than that of Ta-containing alloys. And Ta-containing BMG that is fully amorphous was higher than those that were partially crystalline, due to the presence of the crystalline phase, which hinders the expansion of the plastic region and makes the local plastic region smaller.

5. Conclusions

In this article, a series of $Zr_{60}Cu_{20-x}Al_{10}Ni_{10}M_x$ ($M=Nb$ and Ta , $x=0, 1, 3$, and 5) alloys were prepared. And the primary conclusions of the investigation of these BMGs can be summarized as follows:

- (1) The thermodynamic feature temperature is characterized. The T_g and T_x were reduced during the minor element adding. The containing Nb alloys distinctly improve the plasticity of BMGs and the alloys remain full amorphous structure, the maximum plasticity of adding Nb was 32.9%. And the plasticity was enhanced with the quantity of Ta element and the alloys' structure shifted from compound crystalline-amorphous to full amorphous, and the maximum plastic strain was 9.6%.
- (2) Our results explicitly show the universality of SOC in the BMGs, the power-law distributions for a wide range of the serration event. The high compressive plasticity will be induced by the large rotation angle of the primary SBs. And the yield strength is closely involved in the fracture toughness of BMGs. In this work, the additional minor elements are an effective method for fabricating the BMGs of high structural heterogeneity, in which the inhomogeneous structure of icosahedra-like clusters exhibited the observation of enhanced plasticity.

RediT authorship contribution statement

Ziyun Long, Pingjun Tao and Zhenghua Huang designed the investigation; **Ziyun Long, Guotai Wang, Kunsen Zhu, Yugan Chen, Weijian Zhang and Zhihao Zhao** performed the measurements processed experimental data; **Ziyun Long and Pingjun Tao** wrote most of the initial versions of the text; **Yuanzheng Yang** is responsible for supervising and leading the planning and execution of scientific research activities, including external coaching to the core team. All authors contributed to research strategy, the discussion and interpretation of the results and to the final form of the text and figures. All authors have read and agreed to the published version of the manuscript.

Declaration of Competing Interest

The authors declare that they have no known competing financial interests or personal relationships that could have appeared to influence the work reported in this paper.

Acknowledgment

This work was financially supported by the National Natural Science Foundation of China (51735003, 52071089), the Basic and Applied Basic Research Major Project of Guangdong Province (2019B030302010), the Applied Science and Technology Research Project of Guangdong Province (2015B010127003), the Guangzhou Science and Technology Project (201807010012), the 2019 Guangdong Province Science and Technology Special Fund ("Big Special Project + Task List" Management Mode) Funded Project (2019dzx025) of Qingyuan City, and GDAS' Project of Science and Technology Development (2019GDASYL-0203002). Meanwhile, we would like to thank Analysis and Test Center of Guangdong University of technology for their DSC analysis.

References

- [1] L. Zhang, Y. Huang, X. Cheng, H. Fan, Y. Sun, Z. Ning, F. Cao, J. Sun, Biocompatibility of a micro-arc oxidized $ZrCuAlAg$ bulk metallic glass, *J. Mater. Sci. Technol.* 13 (2021) 486–497, <https://doi.org/10.1016/j.jmrt.2021.04.093>
- [2] W. Lu, M. He, D. Yu, X. Xie, H. Wang, S. Wang, C. Yuan, A. Chen, Ductile behavior and excellent corrosion resistance of Mg-Zn-Yb-Ag metallic glasses, *Mater. Des.* 210 (2021) 110027, <https://doi.org/10.1016/j.matdes.2021.110027>
- [3] J. Jiang, Z.B. Wang, S.J. Pang, Y.G. Zheng, Y. Li, Oxygen impurity improving corrosion resistance of a Zr-based bulk metallic glass in 3.5 wt% NaCl solution, *Corros. Sci.* 192 (2021) 109854, <https://doi.org/10.1016/j.corsci.2021.109854>
- [4] Z. Zhao, J. Mu, H. Zhang, Y. Wang, Y. Ren, Oxygen addition for improving the strength and plasticity of TiZr-based amorphous alloy composites, *J. Mater. Sci. Technol.* 79 (2021) 212–221, <https://doi.org/10.1016/j.jmst.2020.12.005>
- [5] F. Wang, A. Inoue, F.L. Kong, S.L. Zhu, E. Shalaan, F. Al-Marzouki, W.J. Botta, C.S. Kiminami, Yu.P. Ivanov, A.L. Greer, Formation stability and ultrahigh strength of novel nanostructured alloys by partial crystallization of high-entropy $(Fe_{0.25}Co_{0.25}Ni_{0.25}Cr_{0.125}Mo_{0.125})_{86-89}B_{11-14}$ amorphous phase, *Acta Mater.* 170 (2019) 50–61, <https://doi.org/10.1016/j.actamat.2019.03.019>
- [6] R. Farahani, R. Gholamipour, Giant size effect on compressive plasticity of $(Zr_{55}Cu_{30}Al_{10}Ni_5)_{99}Nb_1$ bulk metallic glass, *Mater. Sci. Eng. A* 651 (2016) 948–975, <https://doi.org/10.1016/j.msea.2015.11.063>
- [7] A.Y. Churymov, A.I. Bazlov, A.A. Tsarkov, A.N. Solonim, D.V. Louzguine-Lugin, Microstructure, mechanical properties, and crystallization behavior of Zr-based bulk metallic glasses prepared under a low vacuum, *J. Alloy. Compd.* 654 (2016) 87–94, <https://doi.org/10.1016/j.jallcom.2015.09.003>
- [8] Z.H. Chu, B. Huang, G.Y. Yuan, J. Zhang, J. Yin, W.J. Ding, Microstructure and fracture behavior of $Zr_{55}Cu_{30}Al_{10}Ni_5$ bulk metallic glass and its composites containing ZrO_2 , *Rare Met. Mater. Eng.* 40 (2011) 765–768, [https://doi.org/10.1016/S1875-5372\(11\)60034-9](https://doi.org/10.1016/S1875-5372(11)60034-9)
- [9] F. Farahani, R. Gholamipour, Statistical Weibull analysis of compressive fracture strength of $(Zr_{55}Cu_{30}Al_{10}Ni_5)_{99}Nb_1$ bulk metallic glass, *J. Alloy. Comp.* 695 (2017) 2740–2744, <https://doi.org/10.1016/j.jallcom.2016.11.195>
- [10] K.S. Zhu, P.J. Tao, C.H. Zhang, Z.H. Zhao, W.J. Zhang, Y.Z. Yang, K. Kaviyarasu, Effect of strain rates on the plastic deformation behavior and serrated flow of $Zr_{55.7}Cu_{22.4}Ni_{7.2}Al_{14.7}$ bulk metallic glass, *Mater. Today Commun.* 27 (2021) 102320, <https://doi.org/10.1016/j.mtcomm.2021.102320>
- [11] J.C. Qiao, Q. Wang, J.M. Pelletier, H. Kato, R. Casalini, D. Crespo, E. Pineda, Y. Yao, Y. Yang, Structural heterogeneities and mechanical behavior of amorphous alloys, *Prog. Mater. Sci.* 104 (2019) 250–329, <https://doi.org/10.1016/j.pmatsci.2019.04.005>
- [12] H.K. Kim, J.P. Ahn, B.J. Lee, K.W. Park, J.C. Lee, Role of atomic-scale chemical heterogeneities in improving the plasticity of Cu-Zr-Ag bulk amorphous alloys, *Acta Mater.* 157 (2018) 209–217, <https://doi.org/10.1016/j.actamat.2018.07.040>
- [13] J. Yang, Z. Zhao, J. Mu, Y. Wang, Effect of pre-plastic-deformation on mechanical properties of TiZr-based amorphous alloy composites, *Mater. Sci. Eng. A* 716 (2018) 23–27, <https://doi.org/10.1016/j.msea.2018.01.042>
- [14] R. Qu, R. Maasß, Z. Liu, D. Tönnies, L. Tian, R.O. Ritchie, Z. Zhang, C.A. Volkert, Flaw-insensitive fracture of a micrometer-sized brittle metallic glass, *Acta Mater.* 218 (2021) 117219, <https://doi.org/10.1016/j.actamat.2021.117219>
- [15] Y. Fu, H. Chen, R. Guo, Y. Huang, M.R. Toroghinejad, Extraordinary strength-ductility in gradient amorphous structured Zr-based alloy, *J. Alloy. Compd.* 888 (2021) 161507, <https://doi.org/10.1016/j.jallcom.2021.161507>
- [16] P.J. Tao, W.J. Zhang, Y.G. Chen, J.F. Si, K.S. Zhu, Z.H. Huang, Y.Z. Yang, Effect of high-temperature deformation on the deformation behavior and thermodynamic properties of a Zr-based bulk amorphous alloy, *J. Alloy. Compd.* 907 (2022) 164450, <https://doi.org/10.1016/j.jallcom.2022.164450>
- [17] L.S. Luo, B.B. Wang, F.Y. Dong, et al., Structural origins for the generation of strength, ductility and toughness in bulk-metallic glasses using hydrogen microalloying, *Acta Mater.* 171 (2019) 216–230, <https://doi.org/10.1016/j.actamat.2019.04.022>
- [18] D.W. Ding, J. Tan, A.H. Cai, Y. Liu, H. Wu, Q. An, P.W. Li, Y. Zhang, Q. Yang, Effect of Ti addition on properties of $Zr_{54}Al_{10.2}Ni_{9.4}Cu_{26.4}$ glass-forming alloy, *J. Alloy. Compd.* 864 (2021) 158911, <https://doi.org/10.1016/j.jallcom.2021.158911>
- [19] H. Guan, M. Li, Enhancement of plasticity by cryogenic thermal cycling on $Fe_{80}P_{13}C_7$ bulk amorphous alloy, *Mater. Lett.* 300 (2021) 130195, <https://doi.org/10.1016/j.matlet.2021.130195>
- [20] S.L. Zhang, B. Shi, J.H. Wang, Y.L. Xu, P.P. Jin, Rejuvenation of a naturally aged bulk metallic glass by elastostatic loading, *Mater. Sci. Eng. A* 806 (2021) 140843, <https://doi.org/10.1016/j.msea.2021.140843>
- [21] K.S. Son, X.M. Wang, Y. Yokoyama, K. Yubuta, A. Inoue, Formation, thermal stability, and mechanical properties of glassy $Zr_{60}Cu_{20}Al_{10}Ni_{10}$ alloy rods with diameters of 18 and 20 mm, *Mater. Trans.* 50 (2009) 2021–2027, <https://doi.org/10.2320/matertrans.MRA2008419>
- [22] A. Takeuchi, A. Inoue, Classification of bulk metallic glasses by atomic size difference, the heat of mixing and period of constituent elements and its application to characterization of the main alloying element, *Mater. Trans.* 46 (2005) 2817–2829, <https://doi.org/10.2320/matertrans.46.2817>
- [23] A. van den Beukel, J. Sietsma, The glass transition as a free volume-related kinetic phenomenon, *Acta Metall. Mater.* 38 (1990) 383–389, [https://doi.org/10.1016/0956-7151\(90\)90142-4](https://doi.org/10.1016/0956-7151(90)90142-4)
- [24] L. Liu, C. Qiu, M. Sun, Q. Chen, K. Chan, G.K. Pang, Improvements in the plasticity and biocompatibility of Zr-Cu-Ni-Al bulk metallic glass by the microalloying of Nb, *Mater. Sci. Eng. A* 449–451 (2007) 193–197, <https://doi.org/10.1016/j.msea.2006.02.255>

- [25] T. Li, Y. Liao, S. Song, Y. Jiang, P. Tsai, J. Jang, J. Huang, Significantly enhanced mechanical properties of ZrAlCo bulk amorphous alloy by microalloying with Ta, *Intermetallics* 93 (2018) 162–168, <https://doi.org/10.1016/j.intermet.2017.12.008>
- [26] A. Inoue, T. Shibata, T. Zhang, Effect of additional element on glass transition behavior and glass formation tendency of Zr-Al-Cu-Ni alloys, *Mater. Trans.* 35 (1995) 1420–1426, <https://doi.org/10.2320/matertrans1989.36.1420>
- [27] D.B. Miracle, W.S. Sanders, O.N. Senkov, The influence of efficient atomic packing on the constitution of metallic glasses, *Philos. Mag.* 83 (2003) 2409–2428, <https://doi.org/10.1080/1478643031000098828>
- [28] A. Inoue, Stabilization of metallic supercooled liquid and bulk amorphous alloys, *Acta Mater.* 48 (2000) 279–306, [https://doi.org/10.1016/S1359-6454\(99\)00300-6](https://doi.org/10.1016/S1359-6454(99)00300-6)
- [29] J. Qiao, J. Pelletier, Crystallization kinetics in Cu₄₆Zr₄₅Al₇Y₂ bulk metallic glass by differential scanning calorimetry (DSC), *J. Non-Cryst. Sol.* 357 (2011) 2590–2594, <https://doi.org/10.1016/j.jnoncrysol.2010.12.071>
- [30] L.H. Liu, Z.Y. Liu, Y. Huan, X.Y. Wu, Y. Lou, X.S. Huang, L.J. Li, L.C. Zhang, the effect of structural heterogeneity on the serrated flow behavior of Zr-based metallic glass, *J. Alloy. Compd.* 766 (2018) 908–917, <https://doi.org/10.1016/j.jallcom.2018.07.026>
- [31] X. Sun, J. He, H. Jiang, L. Zhang, J. Zhao, Chemical heterogeneous structure and internal record of deformation behavior in Cu-Fe-Zr metallic glasses, *J. Alloy. Compd.* 886 (2021) 161220, <https://doi.org/10.1016/j.jallcom.2021.161220>
- [32] J. Qiao, P. Liaw, Y. Zhang, Ductile-to-brittle transition of in situ dendrite-reinforced metallic-glass-matrix composites, *Scr. Mater.* 64 (2011) 462–465, <https://doi.org/10.1016/j.scriptamat.2010.11.012>
- [33] A. Greer, Y. Cheng, E. Ma, Shear bands in metallic glasses, *Mater. Sci. Eng. R.-Rep.* 74 (2013) 71–132, <https://doi.org/10.1016/j.mser.2013.04.001>
- [34] G. Wang, K.C. Chan, L. Xia, P. Yu, J. Shen, W.H. Wang, Self-organized intermittent plastic flow in bulk metallic glasses, *Acta Mater.* 57 (2009) 6146–6155, <https://doi.org/10.1016/j.actamat.2009.08.040>
- [35] Z. Wang, J.W. Qiao, H. Tian, B.A. Sun, B.C. Wang, B.C. Xu, M.W. Chen, Composition mediated serration dynamics in Zr-based bulk metallic glasses, *Appl. Phys. Lett.* 107 (2015) 201902, <https://doi.org/10.1063/1.4935834>
- [36] Z.F. Zhang, G. He, H. Zhang, J. Eckert, Rotation mechanism of shear fracture induced by high plasticity in Ti-based nano-structured composites containing ductile dendrites, *Scr. Mater.* 52 (2005) 945–949, <https://doi.org/10.1016/j.scriptamat.2004.12.014>
- [37] X.K. Xi, D.Q. Zhao, M.X. Pan, W.H. Wang, Y. Wu, J.J. Lewandowski, Fracture of brittle metallic glasses: brittleness or plasticity, *Phys. Rev. Lett.* 94 (2005) 125510, <https://doi.org/10.1103/PhysRevLett.94.125510>
- [38] J.L. Wu, W. h Li, Y. Pan, J.Y. Qi, J.G. Wang, Microalloying and microstructures of Cu-based bulk metallic glasses & composites and relevant mechanical properties, *Mater. Des.* 89 (2006) 1130–1136, <https://doi.org/10.1016/j.matdes.2015.10.054>